

CFD Analysis of a Launch Vehicle with Reverse Flow Nozzles-A Validation Study

J Sreenivasulu, Patil M M and A E Sivaramakrishnan
 Vikram Sarabhai Space Center, Thiruvananthapuram, India.
 (sreenivas_j@vssc.gov.in or jksnivas@gmail.com)

Abstract

CFD analysis has been carried out over a typical wind tunnel model Launch Abort System (LAS) Configuration. The viscous turbulent flow studies have been carried out to generate aerodynamic coefficients at Mach 1.6, various angles of attack under jet-on and jet-off conditions using the PARAS-3D code. The present CFD solver is validated using the aerodynamic coefficient of LAS data obtained through CFD and Wind Tunnel experiments. The comparison shows good match with experimental data at lower angles of attack and reasonable match at higher angles of attack under jet-off and jet-on conditions. This study shows that CFD can be applied to predict the aerodynamic coefficients and flow field analysis of launch vehicle with reverse flow jets.

Keywords: Aerodynamic coefficients, PARAS-3D, Jet-off, Jet-on

NOMENCLATURE

<i>CFD</i>	=	Computational Fluid Dynamics
<i>CFL</i>	=	Courant-Friedrichs-Lewy number
<i>LAS</i>	=	Launch Abort System
<i>PARAS</i>	=	Parallel Aerodynamic Simulator
<i>TVD</i>	=	Total Variation Diminishing
<i>WT</i>	=	Wind Tunnel
α/AOA	=	Angle of attack, deg
β	=	Sideslip angle, deg
C_N	=	Normal force coefficient
C_P	=	Coefficient of pressure
C_T	=	Thrust coefficient = $T/q \cdot S_{ref}$
<i>Lref</i>	=	Reference length (0.25 meter)
<i>M</i>	=	Mach number
P_j/P_{inf}	=	Jet Pressure ratio
<i>q</i>	=	Dynamic Pressure, N/m ²
S_{ref}	=	Reference area, m ²
<i>T</i>	=	Thrust, <i>N</i>
<i>Xcg</i>	=	Center of gravity (distance of $0.65 \times Lref$ from the vehicle base), m
<i>Xcp</i>	=	Center of pressure (distance from <i>Xcg</i>), positive direction is from the <i>Xcg</i> toward the base, m

1. INTRODUCTION

Computational Fluid Dynamics constitutes a new “third approach” in the philosophical study and development of the whole discipline of fluid dynamics. It nicely and synergistically complements the other two approaches of pure theory and pure experiments, but it will never replace either of these approaches (as sometimes stated). Computational fluid dynamic results are directly analogous to wind tunnel results obtained in a laboratory. The advancement of fluid dynamics will rest upon proper balance of three approaches, with computational fluid dynamics helping to interpret and understand the

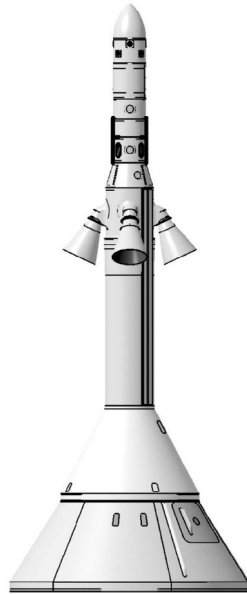


Figure 1. Geometry of Launch Abort System with reverse flow nozzles (Ref.2).

results of theory and experiment, and vice versa [1].

The configuration of a human spaceflight launch aborts system [2, 3] with reverse flow nozzles is shown in Figure 1. As illustrated in Figure 1, two geometry elements dominate the aerodynamic configuration of the LAS reverse flow nozzle configuration. One is the set of nacelles comprising the reverse flow nozzles. The other is the large flare to carry the crew module at the downstream of the rocket nozzles.

The main objective of this study is to demonstrate that CFD can be applied to predict aerodynamic coefficients and flow field features for launch vehicle with reverse flow nozzles in presence of jet. Section two of this paper presents geometry details and computational approach carried out using PARAS-3D. Section three gives the validation and details of the studies carried out at Mach number 1.6 at various angles of attack.

2. COMPUTATIONAL ANALYSIS

2.1. Geometry details

The launch vehicle configuration used in the CFD study consists of an ogive nose followed by a cylinder with propulsive nozzles (4 no's) at the middle of the cylinder, followed by a flare. These unconventional nozzles are of reverse flow type. This configuration has a base diameter of 0.25 m; the total length of configuration is 0.6477 m. Figure 1 shows the LAS with reverse flow nozzles and 3D model for CFD analysis shown in Figure 2.

2.2. Mesh generation

The PARAS code uses the Cartesian grids. The grid is generated by means of an adaptive Cartesian mesh technique. The flow domain is 0.6 m upstream, 2.7 m on the downstream and 2 m on the remaining sides. The initial coarse grid contained nearly 6 million cells and the final finer grid turned out to be 11 million cells. In order to capture the flow features, appropriate cluster was used to make finer grid near the body. Figure 3 shows the section of 3D grids for Mach number 1.6. The boundary conditions are implemented with the dummy cells. Close up view of the computational mesh of the LAS configuration is shown in Figure 4. Final grid after refinement is shown in Figure 5.

2.3. Flow solver

The study has been carried out using Computational Fluid Dynamics (CFD) through an in house

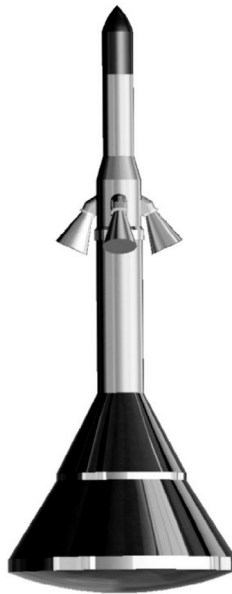


Figure 2. 3D model used for CFD simulation.

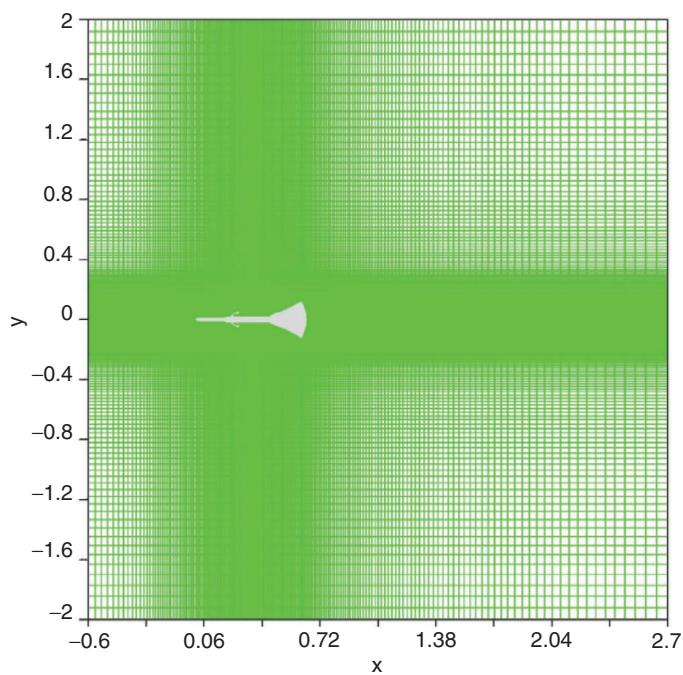


Figure 3. Sectional view of the grid for Mach 1.6.

developed code PARAS-3D. PARAS-3D is a versatile tool for analyzing various type of flow with multiple free streams. The Reynolds Averaged Navier-Stokes (RANS) equations are solved. The turbulent flows are simulated using $k-\epsilon$ model in association with modified wall functions. The time stepping is done for each cell based on local CFL criteria and fluxes at the interface of the cell are

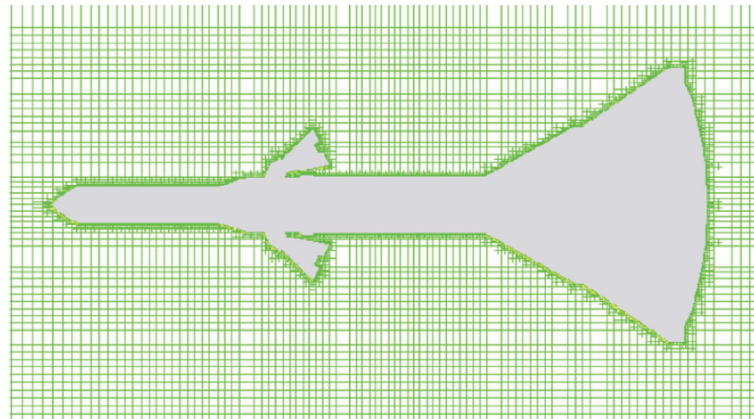


Figure 4. Close up view of the computational grid.

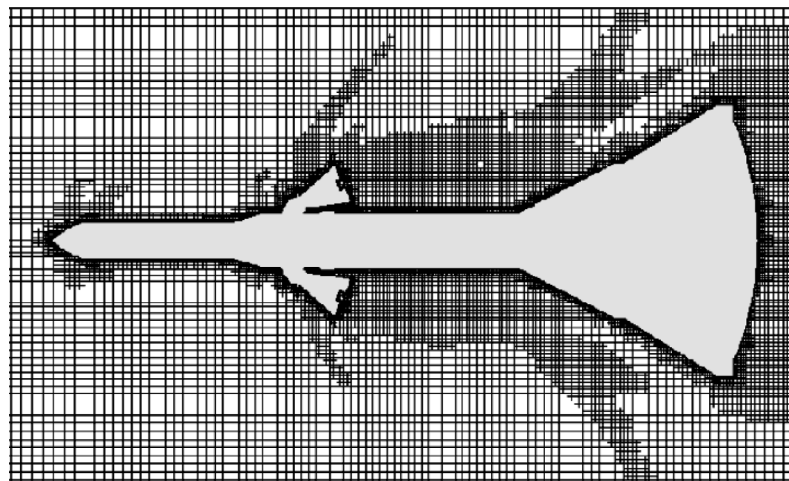


Figure 5. Close up view of the grid after refinement.

computed by means of an approximate Riemann solver. The explicit scheme used is second order accurate in space and of TVD type, which is achieved by means of min-mod limiter. As the solution proceeds, the flow can be refined by adding more grids at regions of high flow gradients and at the same time removing extra cells around regions of low flow gradients.

2.4. Boundary conditions

The CFD simulations are carried out at Mach number of 1.6 and the corresponding Reynolds number. The free-stream static pressure and density corresponds to the wind tunnel conditions are given in Table 1. The jet pressure ratio for the corresponding Mach number is given in Table 2. Studies were made for vehicle angles of attack between 0° to 20°. Upwind boundary conditions are used for inward flow and shift (zero flow gradients) for all remaining surfaces. For jet-on condition, exit properties are applied at the exit of

Table 1. Free stream condition for simulation

M	1.6
Pressure (N/m ²)	48349.8
Density (Kg/m ³)	0.673092
Angle of attack (deg)	0 to 20°

Table 2. Jet pressure ratio for jet-on condition

M	(P_j/P_{inf})
1.6	6.52

the nozzle.

2.5. Convergence criteria

The main convergence criteria [4] used to monitor and determine solution convergence is given below:

Convergence of force and moment coefficients was evaluated with a percent over a range (%OR) value of less than 1 percent for each coefficient. The %OR value was calculated with Eq. (1), where CNmax is the value of the coefficient at the last iteration. The coefficients were averaged over 10000 iterations. The standard deviation and %OR value is calculated for each coefficient.

$$\%OR = \frac{C_{N_{max}} - C_{N_{max-9999}}}{C_{ave}} \times 100\% \tag{Eq. (1)}$$

$$\text{Where: } C_{ave} = \frac{1}{10000} \sum_{j=N_{max}-9999}^{N_{max}} C_j$$

A typical convergence and grid independence plot in Figure 6 shows the convergence of normal force coefficients for LAS configuration at Mach 1.6, AOA of 20° under jet-on condition. For various grid sizes the solution converged very well (with 0.5% variation).

2.6. Computer platform

All simulations were done at the SAGA-220 (Supercomputer for Aerospace with GPU Architecture), at Shatish Dhawan Super Computing Facility, VSSC. It operates with in house developed Compute Node Linux 2.0 (64-bit) supporting GPU & Infiniband. The facility is powered by NVIDIA Tesla

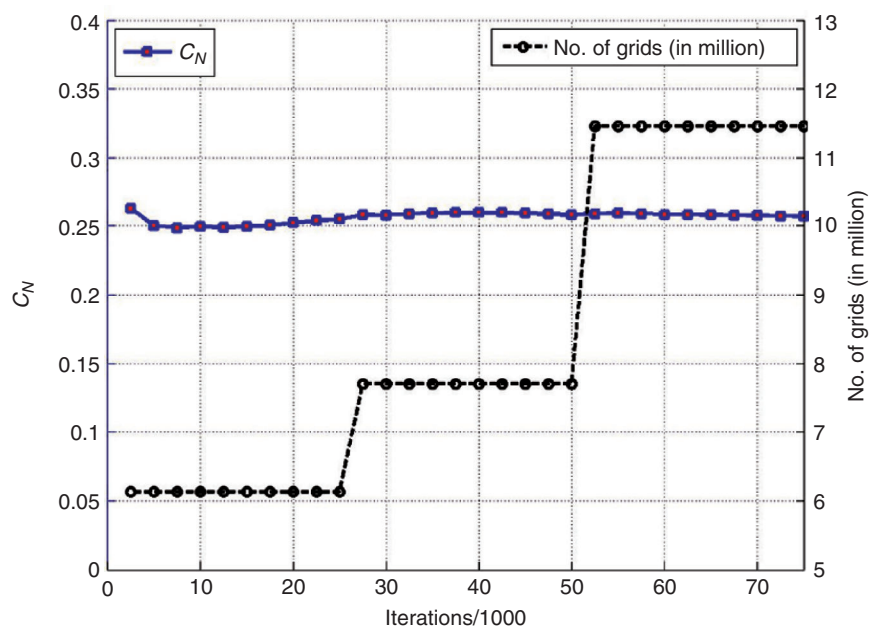


Figure 6. Normal force coefficient convergence & grid independence plot for LAS at angle of attack of 20° under jet-on ($C_T = 0.34$) condition.

C2070 GPU (FERMI). The PARAS-3D flow solver uses approximately 0.101 $\mu\text{sec}/\text{cell}/\text{iteration}$ on a single GPU for finer grid. Each solution used 6 GPU'S in parallel to solve the flow equations.

3. RESULTS & DISCUSSION

The viscous simulation tool used in this study is validated using existing wind tunnel test [3] & CFD data [2]. The wind tunnel experiment [3] provided opportunities to understand the flow physics of LAS with reverse-flow motors and to verify the CFD predictions, both qualitatively and quantitatively. The CFD results are verified by using 1) surface pressure measurement 2) Aerodynamic coefficients 3) Flow visualization.

The surface pressure measurements (Figure 7) are used to verify the CFD pressure distribution along the launch vehicle body. Results (Figure 7) indicate that surface pressure predictions are in very good agreement with WT measurement data [3].

The aerodynamic coefficients are calculated based on the ref. length of 0.25 m and ref. area of 0.049 m^2 .

(a) Mach 1.6, jet-off condition ($C_T = 0$)

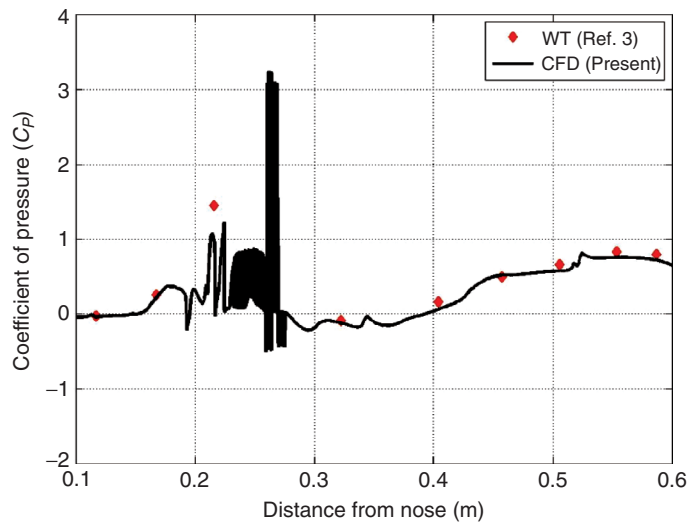


Figure 7. C_p distribution over LAS configuration at angle of attack of 20° in presence of jet ($C_T = 0.34$).

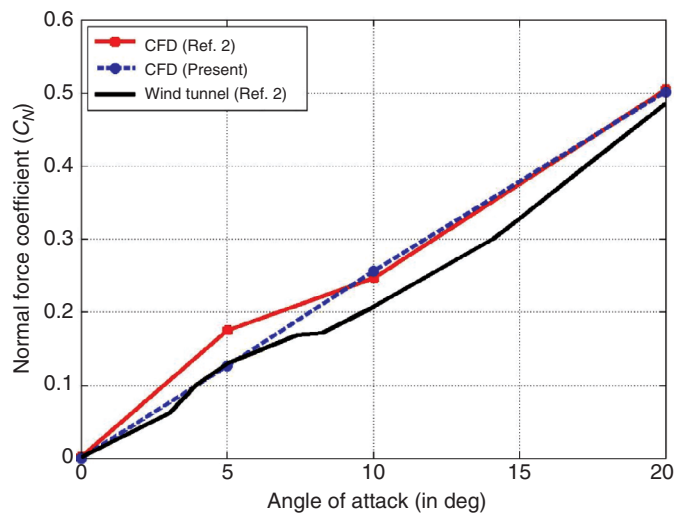


Figure 8. Normal force coefficient for LAS configuration at various angles of attack under jet-off ($C_T = 0$) condition.

Comparison of normal force coefficient with various angles of attack is shown in Figure 8. The comparison indicates that the present CFD data gives good match with WT data at lower angles of attack compared to CFD reported [2]. As the angle of attack increases normal force coefficient increases. Figure 9 shows the variation of non-dimensionalized center of pressure with AOA. Figure 9 shows the present CFD results are good agreement with WT reported data at AOA of 5° & 20° and large variation at AOA of 10° is observed. It may be due to unsteadiness in the flow. As the angles of attack increases center of pressure moves towards the nose due to increase in the normal force coefficient. From Figure 9 Present CFD & reported CFD [2] simulations show that the vehicle is statically stable under jet-off condition till 10° angle of attack, whereas WT [2] data shows the vehicle stable around 5° angle of attack. In Figure 9 as angle of attack increases from 5° to 10°, reported CFD and WT [2] data shows the center of pressure decreases, whereas present CFD shows the constant trend it may be due to unsteadiness in the flow.

(b) Mach 1.6, jet-on condition ($C_T = 0.34$)

Comparison of normal force coefficient, variation of non-dimensionalized center of pressure with various angles of attack as shown in Figure 10 & Figure 11. Figures indicate a good match between WT [2] data

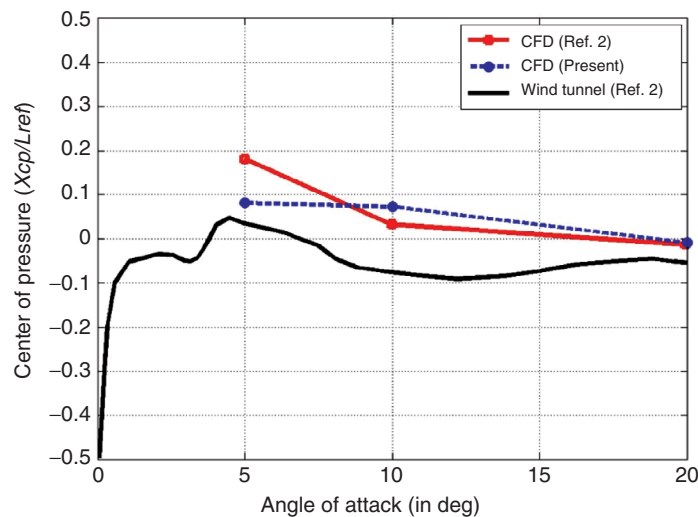


Figure 9. Center of pressure variation for LAS configuration at various angles of attack under jet-off ($C_T = 0$) condition.

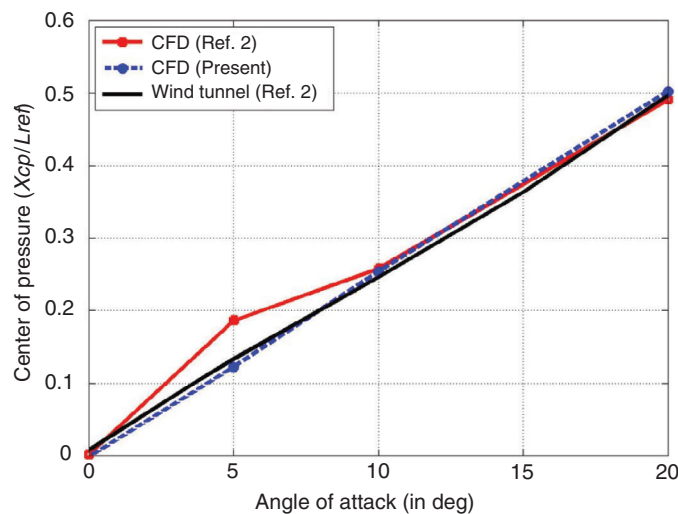


Figure 10. Normal force coefficient for LAS configuration at various angles of attack under jet-on ($C_T = 0.34$) condition.

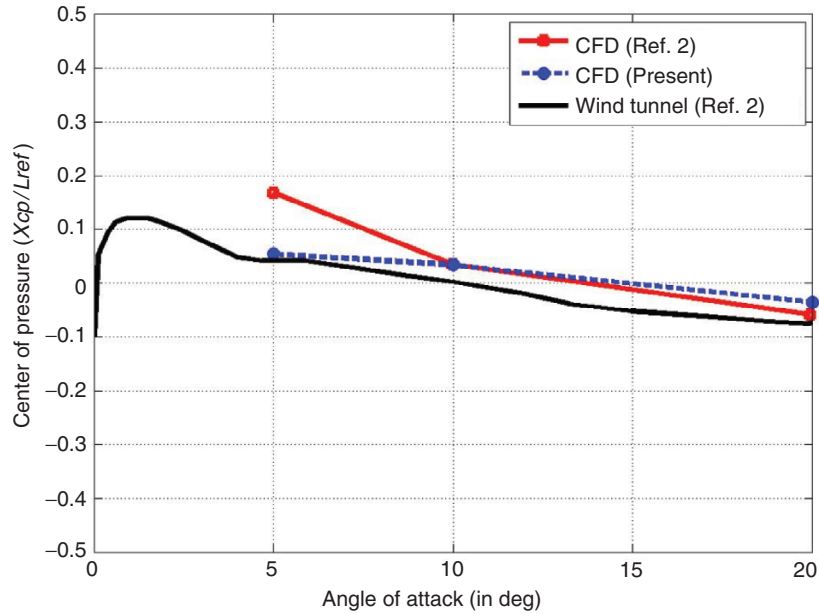


Figure 11. Center of pressure variation for LAS configuration at various angles of attack under jet-on ($C_T = 0.34$) condition.

and present CFD data under jet-on condition. Present CFD code gives the good match compared to CFD reported data [2]. From Figure 11, Present CFD simulations show that the vehicle is statically stable under jet-on condition till 10° angle of attack and statically unstable for angles of attack greater than 10° .

Flow field analysis has been carried out at Mach 1.6, various angles of attack under jet-off and jet-on conditions. Figure 12(a) & (b) shows the comparison of CFD flow visualization and WT [3] using Schlieren visualization technique at Mach 1.6, angle of attack of 0° under jet-off & jet-on ($C_T = 0.34$) conditions. In Figure 12(a) & (b) top half of the figure shows the WT Schlieren photograph, bottom half shows the present CFD flow field. The figure indicates that the CFD code captures flow features like bow shock at the nose cone region, oblique shock at first flare region, expansion fan at the end of the first flare. Oblique shocks at the nozzle and flare region are also captured well. Velocity vectors over LAS leeward nozzle section plane at Mach 1.6, AOA of 0° under jet-off and jet-on conditions are shown in Figure 13. Figure 13 (a) shows jet-off condition, where the separation of the flow at the nozzle region can be observed and Figure 13 (b) shows the jet-on condition, where the flow emanating from the nozzle exit can be seen clearly. Figure 14 shows the comparison of flow visualization using WT

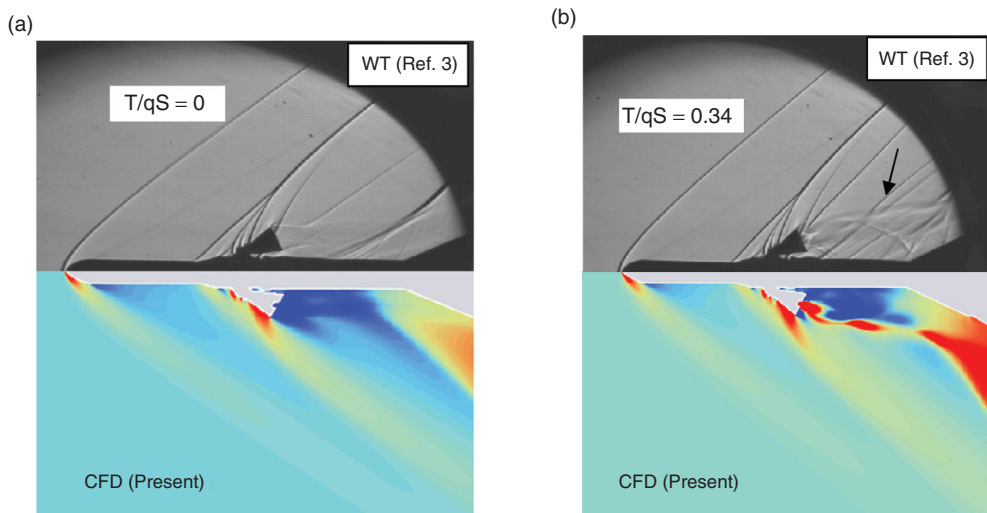


Figure 12. Comparison of WT & CFD flow features (a) jet-off (b) jet-on ($C_T = 0.34$) condition.

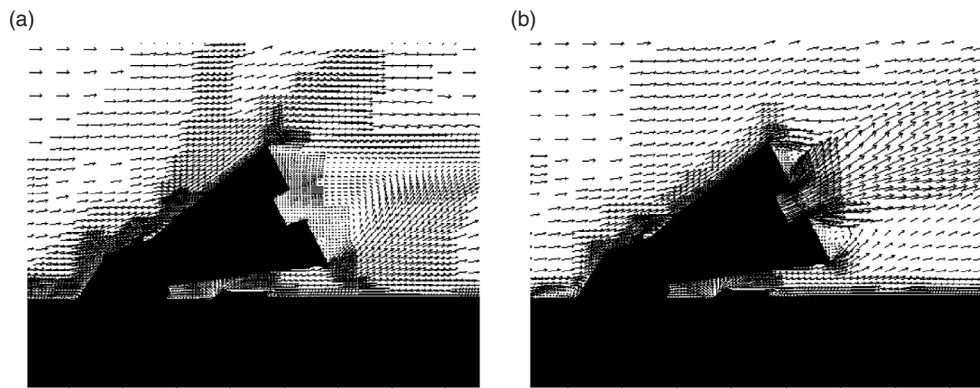


Figure 13. Velocity vectors over nozzle at Mach 1.6, $\alpha = 0^\circ$ (a) jet-off (b) jet-on condition.

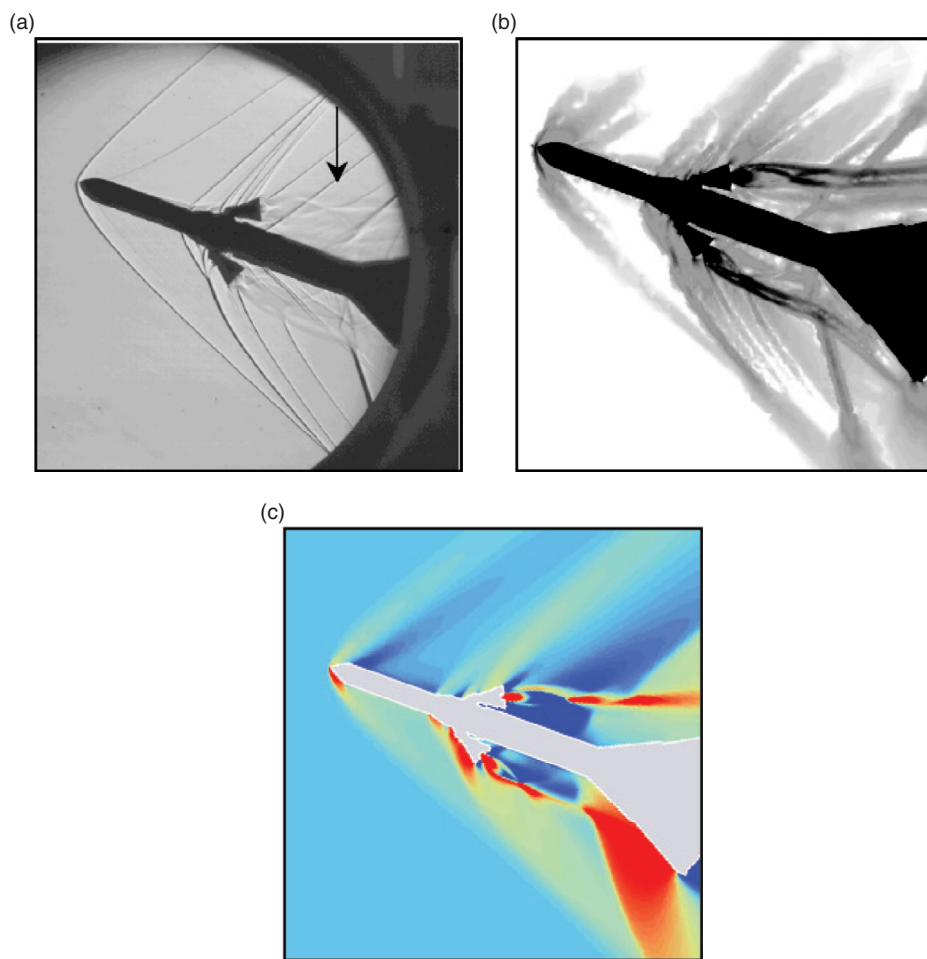


Figure 14. Comparison of flow features (a) WT Shadowgraph (Ref.2) (b) CFD (Ref.2) (c) CFD (Present) showing magnitude of density gradients.

Schlieren photograph [2], CFD flow field density gradients [2] and present CFD in the pitch plane at Mach 1.6 and AOA of 20 under jet-on condition. The complexity of shock like the first-flare shock interacting with the nozzle shock, oblique shock sitting upstream of the plume, and a stronger oblique shock upstream of the second flare, at the windward side are captured well. In Figure 12 (b) and Figure 14 the oblique shock downstream of the upper nozzle is clearly seen in WT Schlieren indicated (showed by an arrow), whereas such oblique shock is not seen in the CFD flow field graph. This is because the

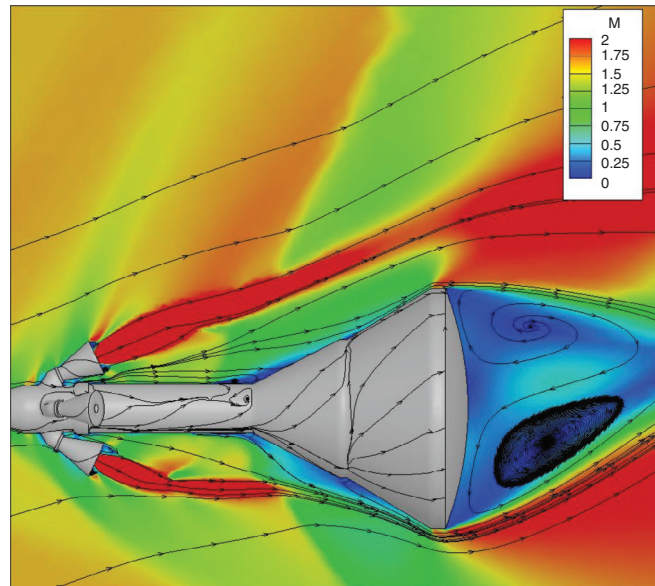


Figure 15. Stream lines over the LAS geometry and flow field at Mach 1.6 and angle of attack of 20°.

WT Schlieren image shows a projection [2] of the entire 3D flow structure into one plane, whereby the CFD shows sectional cut plane view at the center.

Figure 15 shows the streamlines over LAS and in the flow field at Mach 1.6 and angle of attack of 20°. Streamlines at the end of the LAS cylinder portion shows the flow separation. At the base of LAS, wake region is observed clearly.

4. CONCLUSION

Aerodynamic analysis has been carried out over LAS configuration at Mach 1.6, at various angles of attack under jet-off and jet-on conditions. The present CFD code captures the flow characteristics reasonably well. The aerodynamic coefficients and pressure distribution are in good agreement with reported data. The present CFD code can be used for launch vehicle aerodynamic analysis with reverse flow nozzle. The present study brings the application of PARAS-3D code for launch vehicle with reverse flow nozzles.

ACKNOWLEDGMENT

Authors are thankful to Dr. George Joseph., former GD, ADTG and Dr. S.Swaminathan, former Deputy Director, Aeronautics Entity, VSSC for their guidance and encouragement for this work. We are also thankful to Sri. Rakesh C K, HSP for his support in geometry modeling. Authors are thankful to Sri. Harichand & Sri. T C Babu, APCF for their support during simulation work. Authors are also thankful to Sri. K Kumar, DPD, HSP for kindly agreeing to review the paper and for the valuable suggestions.

REFERENCES

- [1] John D. Anderson Jr., "Computational Fluid Dynamics", McGraw-Hill, Inc.
- [2] H. Feiz, L. Glatt, M. Emerick, and S. Kovacic., "CFD Applications to Launch Vehicles with Reverse Flow Plumes", 46th AIAA Aerospace Sciences Meeting and Exhibit, 7–10 January 2008, Reno, Nevada.
- [3] L. A. Cassel, T. P. Shivananda, H. Feiz, S. Kovacic, and R. Douglas, "Reverse Flow Plume Interference Wind Tunnel Testing - For CEV Launch Abort System (LAS)," *AIAA-2008-0347*.
- [4] Karen A. Deere, S. Paul Pao, and Khaled S. Abdol-Hamid., "Computational Analysis of Ares I Roll Control System Jet Interaction Effects on Rolling Moment", *AIAA-2011-172*.